University of Sistan and Baluchestan

Challenges in Nano and Micro Scale Science and Technology

Online ISSN: 2821 - 000X

Thermoelectric Power Enhancement via CNT Microfins: A Computational Approach

Mitra Salami[1]| Tahereh Fanaei Sheikholeslami[2]✉

1. Department of Electrical and Electronic, University of Sistan and Baluchestan, Zahedan, I.R. Iran
2. Department of Mechanical Engineering (Mechatronics), University of Sistan and Baluchestan, Zahedan, I.R. Iran

Article Info

Article type:
Research Article

Keywords:
Thermoelectric generator,
CNT,
Heat transfer enhancement,
Thermopile

ABSTRACT

Thermoelectric (TE) devices offer a promising approach to harvesting wasted thermal energy from fluid flow without mechanical components. However, their performance is highly dependent on the of heat transfer between the TE legs and heat sinks, especially under varying fluid temperatures. This study investigates the enhancement of thermal performance at the leg/heat sink interface by integrating carbon nanotube (CNT) arrays as microfins on polymeric TE legs. A validated finite element model is used to simulate device behaviour and assess the impact of CNT geometry and fluid flow conditions. Simulation results reveal that CNT arrays significantly increase the temperature gradient across the TE legs, leading to improved energy conversion rates. Compared to devices without CNTs, the CNT-based thermopile exhibits 1.4 to 2 times higher open-circuit voltage and output power efficiency. When five TE units are connected to form a thermopile, the output reaches 7 mV and 0.3 µW approximately tenfold the performance of a single device. The amount of recovered waste heat from the hot flow source is about 0.0117 W. Optimal power output is achieved through impedance matching, which can be tuned by configuring the number of TE units in series or parallel. These findings highlight the potential of CNT-enhanced TE devices for efficient thermal energy harvesting in fluidic systems.

Nomenclature

C	Heat capacity at constant pressure(J/kgk)	V	Electrical Voltage (v)
E	Electrical Field (v/m)	u,v and w	Velocity at x, y and z direction
J	Flux of Electrical Current (A/m^2)	ZT	Figure of merit
k	Thermal Conductivity (W/mk)		
P	Peltier Coefficient (v)	**Greek symbols**	
p	Pressure (Pa)	α	Thermal Diffusivity (m^2/s)
Q	Joule Heating (J)	μ	Thomson Coefficient (µv/K)
q	Heat Flux (W/m^2)	ρ	Density (kg/m^3)
S	Seebeck coefficient (µv/K)	ρ_c	Space charge density (C/m^2)
T	Temperature (K)	σ	Electrical Conductivity (S/m)
t	Time (s)		

INTRODUCTION

Thermoelectric (TE) devices have emerged as promising energy harvesters for various applications due to their remarkable properties, including long lifespan, noiseless operation, ease of maintenance, and high reliability. Their environmentally friendly impact and straightforward implementation further enhance their appeal. TE devices enable the harvesting of electrical energy from low-grade heat sources, such as human body temperature or the exhaust gas pipe of a vehicle [1]. The harvested electrical energy can be sufficient to power various sensors and control apparatuses.

A TE device consists of two legs- n-type and p-type - composed of distinct TE materials, electrically connected

How to Cite this paper: Salami M. Fanaei Sheikholeslami T. Thermoelectric Power Enhancement via CNT Microfins: A Computational Approach. *Challenges in Nano and Micro Scale Science and Technology*. 2024; 12(2): 72-80. DOI: 10.22111/cnmst.2025.53937.1270

 Publisher: University of Sistan and Baluchestan.
DOI: 10.22111/cnmst.2025.53937.1270

via a conductive material. Thermoelectric generators (TEGs) can be deployed for a range of applications, including waste heat recovery. Notable examples include efforts to convert vehicle exhaust heat into clean electrical energy [2, 3].

However, the low efficiency of TE technology remains a significant challenge that must be addressed to enable widespread adoption. As Bell [4] pointed out, this issue can be tackled by enhancing the intrinsic energy-conversion efficiency of TE materials and integrating the latest advancements in system architecture and design. Current TE generators operate at an efficiency below 5% [5].

Modeling and simulation of TEGs offer a powerful approach for exploring novel strategies to improve performance. Consequently, extensive research has been conducted to simulate various TE devices.

Among these studies, Lu et al. [6] investigated the cooling and mechanical performance of a trapezoidal thermoelectric cooler using the finite element method to simulate a full-scale three-dimensional model. Compared to conventional rectangular designs, they demonstrated that increasing the leg height and employing a variable cross-sectional design enhanced cooling performance. Furthermore, while a greater leg height improved mechanical reliability, the trapezoidal shape negatively impacted it.

Şişik and LeBlanc [7] numerically examined the thermal and electrical performance of TE devices with different leg geometries, including rectangular, hollowed prisms, trapezoidal, hourglass, and Y-shaped legs. Their findings revealed that an hourglass-shaped thermoelectric leg provided superior performance under constant hot-side temperature conditions, achieving more than twice the electrical potential of conventional rectangular legs.

Rjafallah et al. [8] conducted numerical investigations on the effects of leg geometry on TE performance using the finite element method. They studied several shapes, including square, triangular, trapezoidal, reverse trapezoidal, hourglass, and inverse hourglass configurations with varying dimensions. Their results indicated that triangular legs with internal hollows yielded the highest maximum power output.

Ali et al. [9] numerically simulated a thermoelectric generator designed to harvest waste heat from chimneys. Their study comprehensively described heat transfer along a single vertical bar within the TEG module mounted against a chimney wall. Additionally, they analyzed the influence of flap dimensions—height, depth, and angle—alongside the performance of various conductive materials. Mohamed et al. [10] investigated waste heat recovery from the exhaust stream of the main oven in a bakery factory using TE modules. They showed that Reynolds number of stream is the major operating parameter because of its effects on the heat sink effectiveness. They achieved to an increase of heat recovery ratio from an initial 14% to 38%.

Harb et al. [11] employed genetic algorithms to optimize thermoelectric generators, focusing on electricity production and conversion efficiency as key performance metrics. They found that leg length and cross-sectional area significantly influenced energy generation. Alghamdi et al. [11] applied finite element methods to simulate segmented variable-area-leg TE modules, optimizing their design using Bayesian regularized neural networks.

Lin et al. [13] explored the heating and cooling performance of TE devices for medical storage applications. Their optimization study revealed that U-shaped cooling fins significantly enhanced cooling efficiency under specific conditions. Pang et al. [14] developed an analytical 3D mathematical model to examine TEG performance, simplifying complex 3D heat conduction into a more manageable 1D representation through minor adjustments to classical TEG theory.

Dziurdzia et al. [15] proposed an electrothermal model to simulate energy harvesting processes across different TEG scales. Their model accounted for steady and transient states, incorporating variations in electrical loads and temperatures. Kayabaşi and Kaya [16] experimentally showed that using a combination of photovoltaic and TE modules can harvest 0.45V energy output when the TE naturally cooled. It is enhanced to 0.97V energy output when forced-cooled. Yang et al. [17] conducted a systematic review of thermoelectric generators at different scales, discussing technological characteristics at various power levels (microwatt to kilowatt systems). Their research introduced a comprehensive design framework, addressing material innovations and large-scale integration to advance next-generation TE systems.

Polymeric TE devices have attracted significant interest due to their advantages, including large surface area, device flexibility, low cost, low density, low thermal conductivity, and straightforward synthesis [18]. The efficiency of TE systems is heavily dependent on the quality of heat transfer between the heat source and the TE material. Thus, enhancing heat transfer is a critical issue that must be carefully addressed. One effective method involves the use of microfin structures composed of aligned multiwalled carbon nanotubes (CNTs), which exhibit exceptional thermal conductivity [19-21]. However, CNT conductivity is highly anisotropic, with much greater heat transfer efficiency along the nanotube axis compared to other directions.

Current TE research is primarily focused on fabrication methodologies and the development of novel materials to reduce device size and cost [22]. Sun et al. [23] introduced a polymeric TE module featuring 35 legs, capable of generating an output voltage of up to 0.26 V—sufficient to power electronic components within a wireless system.

Increasing the temperature difference across TE device terminals remains a key strategy for enhancing output voltage while minimizing the number and size of legs. Nanostructured interfaces based on vertically aligned CNTs offer an optimal blend of mechanical compliance and high thermal conductance, improving TE device efficiency [21]. Nuwayhid et al. [24] studied a hybrid system of photovoltaic and thermoelectric modules. They concluded that hybridizing a PV panel by bottoming it with a thermoelectric generator is not quite attractive except possibly at higher solar concentrations. However, they

mentioned that further work on this line may include more TE material considerations, and more rigorous heat sink treatment. This study aims to improve the performance of heat sink.

Despite extensive research on TE device fabrication, comparatively fewer studies have focused on modeling complete TE systems. Notably, the integration of CNT electrodes—thermally connecting hot and cold working fluids to TE materials—has not been explored in depth. CNTs also function as microfins, significantly enhancing heat transfer efficiency. This study numerically investigates a novel TE design incorporating vertically aligned CNTs integrated with device electrodes, aiming to improve heat exchange between the legs and the heat sink flow channels.

A finite element technique is used to simulate the proposed polymeric TE device, with a particular focus on the role of CNTs in enhancing heat transfer efficiency. Two configurations are considered and compared: one without CNT integration and another featuring CNT arrays.

Mathematical Formulations

Figure 1 presents a schematic representation of the two thermoelectric (TE) devices considered for simulation. The first configuration, shown in Figure 1a, is a conventional TE device without carbon nanotubes (CNTs). This setup consists of p-type and n-type legs, two electrodes, and two rectangular channels responsible for directing hot and cold gases as heat sources and sinks. Efficient heat exchange between the gas and electrodes is a critical factor influencing the overall performance of the TE device.

To address this, the second configuration integrates conventional electrodes with CNT arrays, as illustrated in Figure 1b. In this model, CNTs function as high-performance microfins, significantly enhancing heat transfer between the gas flow and the TE legs. A total of twenty-seven microfins, each composed of CNT arrays, are strategically positioned on the electrodes within the channels. These microfins not only improve thermal conductivity but also contribute to fluid flow perturbation, further increasing the rate of heat transfer.

For simulation purposes, the microfins are treated as a bulk medium with an effective density of 350 kg/m³ and a specific heat capacity of 650 J/kg·K. The effective anisotropic thermal conductivity of the microfins is represented using the following matrix [20, 25-27].

$$k = \begin{pmatrix} 40 & 40 & 40 \\ 40 & 40 & 40 \\ 40 & 40 & 400 \end{pmatrix}$$

The efficiency of a thermoelectric (TE) material is determined by its dimensionless TE figure-of-merit (ZT), which is mathematically defined as:

$$ZT = (S^2\sigma)T / k \quad (1)$$

Where σ represents electrical conductivity and k denotes thermal conductivity. Therefore, an ideal thermoelectric (TE) material exhibits high electrical conductivity and low thermal conductivity. Based on the characteristics of organic TE materials, polyaniline (PANI) and poly(3,4-ethylenedioxythiophene): poly(styrenesulfonate) (PEDOT: PSS) are selected as the p-type and n-type legs, respectively. Tables 1 and 2 provide details on the material properties and device specifications for both architectures [28-30].

The Seebeck and Peltier effects play a crucial role in the performance of any thermoelectric (TE) device. According to the Seebeck effect, the output voltage of a TE device is determined by the following equation [19]:

$$V = (S_p - S_n)\Delta T \quad (2)$$

where Sp and Sn are Seebeck coefficients of p and n type legs, respectively, and ΔT is temperature difference between both sides of the device.

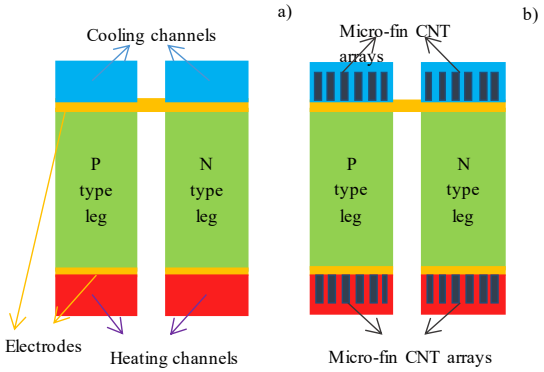

Fig. 1. Schematic of the simulated TE device (a) without CNTs, (b) with CNTs).

Table 1
Materials, and their corresponding size of the TE device.

		Elements	
Properties	Thermoelectric material	Electrode	Thermal interface material
Material	PEDOT:PSS, PANI	Copper	CNT Arrays
Dimension (μm)	900×2000×5000	900×2000×200	100×100×650

Table 2
Physical properties of the considered materials.

Materials	k (W/m k)	σ (S/m)	C (J/kg k)	S_p or S_n (μV/k)	ρ (kg/m³)
PANI	0.53	370	324.56	177	1150
PEDOT:PSS	0.2	930	200	-57	1000
Copper	401	58.1×10^6	384	1.8	8960

These effects are thermodynamically related by the Thomson relations [32]:

$$P = ST \quad (3)$$

$$\mu = T\frac{dS}{dT} \quad (4)$$

where P is the Peltier coefficient and μ is the Thomson coefficient. In a leg of TE device, the heat flux, $\boldsymbol{q}$, and the

flux of electric current, J, are determined by (Xuan et al. 2002) [33]:

$$q = -k\nabla T + PJ \quad (5)$$
$$J = -\sigma\nabla V - \sigma S\nabla T \quad (6)$$

Some other associated quantities are:

$$E = -\nabla V \quad (7)$$
$$Q = J.E \quad (8)$$

where $\boldsymbol{E}$ is the electric field and Q is the Joule heating. Conservation of heating energy and current gives:

$$\rho C\frac{\partial T}{\partial t} + \nabla.q = Q \quad (9)$$
$$\nabla.J = -\frac{\partial \rho_c}{\partial t} \quad (10)$$

In these equations, ρ is the density, C is the heat capacity at constant pressure and ρ_c is the space charge density. At the steady state condition, the above mentioned equations can be simplified as follows:

$$\nabla.q = Q \quad (11)$$
$$\nabla.J = 0 \quad (12)$$

To be able to determine the electrode temperature and consequently

the heat flux at the interface of electrode and TE material, the governing equations for the fluid flow through rectangular channels (heat source and sink) are solved. These governing steady state equations for laminar flow regime are [26]:

Continuity equation:

$$\frac{\partial u}{\partial x} + \frac{\partial v}{\partial y} + \frac{\partial w}{\partial z} = 0 \quad (13)$$

Momentum equations:

$$u\frac{\partial u}{\partial x} + v\frac{\partial u}{\partial y} + w\frac{\partial u}{\partial z} = -\frac{1}{\rho}\frac{\partial p}{\partial x} + v\left(\frac{\partial^2 u}{\partial x^2} + \frac{\partial^2 u}{\partial y^2} + \frac{\partial^2 u}{\partial z^2}\right)$$
$$u\frac{\partial v}{\partial x} + v\frac{\partial v}{\partial y} + w\frac{\partial v}{\partial z} = -\frac{1}{\rho}\frac{\partial p}{\partial y} + v\left(\frac{\partial^2 v}{\partial x^2} + \frac{\partial^2 v}{\partial y^2} + \frac{\partial^2 v}{\partial z^2}\right)$$
$$u\frac{\partial w}{\partial x} + v\frac{\partial w}{\partial y} + w\frac{\partial w}{\partial z} = -\frac{1}{\rho}\frac{\partial p}{\partial z} + v\left(\frac{\partial^2 w}{\partial x^2} + \frac{\partial^2 w}{\partial y^2} + \frac{\partial^2 w}{\partial z^2}\right)$$

Energy equation:

$$u\frac{\partial T}{\partial x} + v\frac{\partial T}{\partial y} + w\frac{\partial T}{\partial z} = \alpha\left(\frac{\partial^2 T}{\partial x^2} + \frac{\partial^2 T}{\partial y^2} + \frac{\partial^2 T}{\partial z^2}\right)$$

Boundary Conditions

Incompressible laminar air flow through the channels is considered, with integrated carbon nanotubes (CNTs) at the channel-electrode interface functioning as microfins. The no-slip boundary condition is applied, while wall radiation and interfacial resistance are neglected. The air flow temperature at the inlet of the hotter and colder channels is set at T_{ih} = 37°C and T_{ic} = 20°C, respectively. The fluid inlet velocity varies between 0.1 m/s and 0.8 m/s, corresponding to Reynolds numbers ranging from 6.31 to 50.52.

Grid Study and Validation

The nonlinear governing equations are discretized using the finite element technique, and the resulting equations are solved using SIMPLE algorithm. An unstructured mesh distribution is employed (see Fig. 2). To ensure grid independence of the calculated results, multiple grid distributions have been tested. Fig. 3 illustrates the effect of grid resolution on the temperature difference between the two legs for both models. In the first model (without CNTs), increasing the grid number beyond 13,435 does not significantly affect the results. In contrast, for the second model (with CNTs), grid independence is achieved at 142,700. The second model requires a higher mesh resolution than the first due to the presence of microfin CNTs.

To demonstrate the validity and accuracy of the mathematical model and numerical procedure, the output voltage of the TE device, calculated at different temperature differences between the two ends of the leg, is compared with the corresponding experimental results obtained by Wang et al. [34]. As shown in Fig. 4, agreement between the numerical and experimental results is observed. As can be seen, the difference between the results is smaller at lower temperature differences. This difference varies approximately between 5 and 20 percent. This confirms that the numerical procedure is reliable and capable of accurately predicting the TE performance.

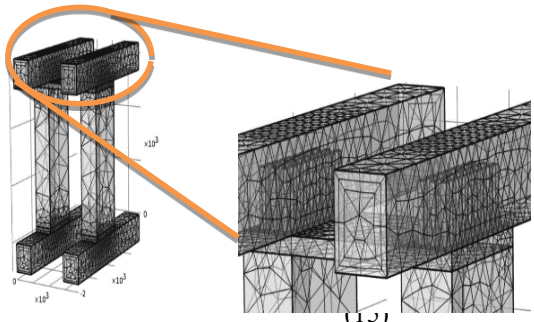

Fig. 2. 3D unstructured grid for modelling the TE device using CNT arrays.

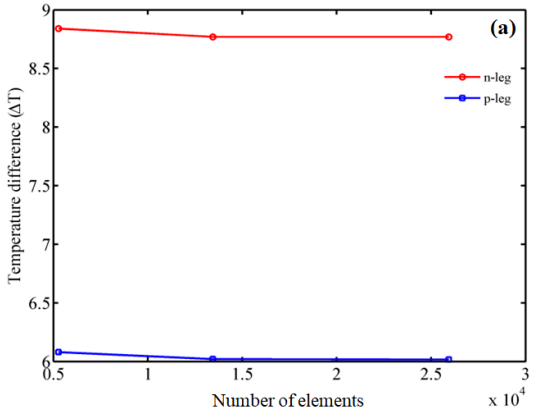

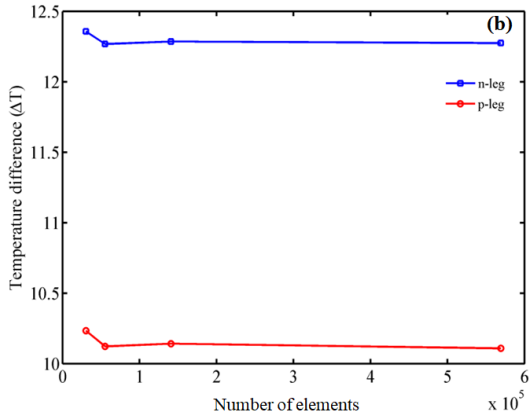

Fig. 3. Grid test (a) TE without CNTs (b) TE with CNTs

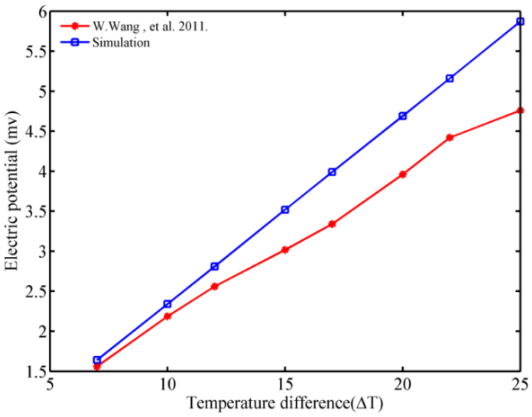

Fig. 4. A comparison of TE device output voltage between the present numerical result and experimental results of Wang et al. [34]

RESULTS AND DISCUSSIONS

It is well known that the performance of a TE device strongly depends on the temperature difference between the two ends of its legs. Therefore, enhancing heat transfer at the junctions between the legs and the heat source and sink (hot and cold gas flow through the channels) is crucial for achieving a higher temperature at the hotter zone and a lower temperature at the colder zone.

To examine the effect of CNTs on temperature variations along the device legs, Fig. 5 is presented. As observed, for given Reynolds numbers (fluid velocity) and air temperatures at the channel inlets, the use of CNTs results in a greater temperature difference in both p-type and n-type legs, thereby improving the device's performance. This enhancement occurs because CNTs simultaneously increase the effective heat transfer surface in contact with the airflow and disturb the fluid flow. These effects significantly enhance heat transfer between the airflow and the electrodes, leading to a higher temperature at the heat source and a lower temperature at the heat sink.

A comparison between the two TE models reveals that the temperature difference in the second model (which utilizes CNTs) is 1.5 times greater than that of the first model. Additionally, the temperature difference across the n-type leg is higher than that of the p-type legs due to the lower thermal conductance of PEDOT:PSS under identical conditions. It is worth noting that microstructured, etched CNT films used as microfins exhibit a more effective heat transfer behavior than unetched CNT films [17]. This improvement is attributed to the presence of grooves that facilitate better fluid flow and heat dissipation through convective fluxes from the fins to the surrounding medium.

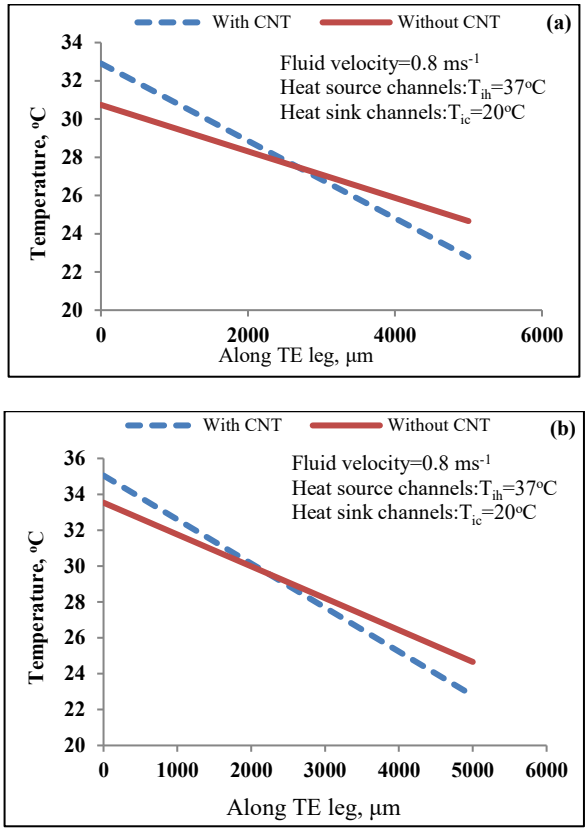

Fig. 5. Variations of temperature along TE legs (a) p and (b) n type for TE with and without CNTs

However, the present model considers the CNT arrays as a solid block, whereas in reality, CNTs consist of numerous hydrophilic strands that intertwine and entangle, forming nanoscale pores that allow fluid penetration and further enhance heat transfer efficiency

It is well known that the dimensions of the legs and the inlet gas flow conditions at the heat source and sink channels significantly influence the performance of a thermoelectric device. Fig. 6 illustrates the impact of leg height on temperature differences and open-circuit voltage for thermoelectric devices with and without CNTs.

As observed, increasing the leg height leads to greater thermal resistance between the leg sides, which in turn enhances the temperature difference and consequently raises the open-circuit voltage. However, this variation does not follow a linear trend, as the rate of temperature difference increase diminishes with further leg height expansion.

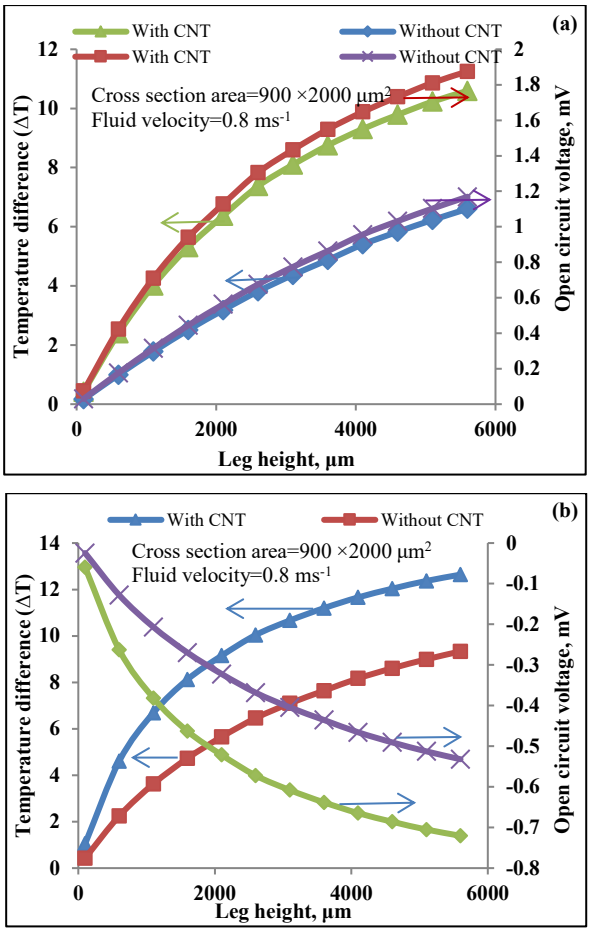

Fig. 6. The effect of legs height on the temperature differences and open circuit voltages for a given velocity for TE with and without CNTs (a) p and (b) n type legs. T_{ih}=37°C and T_{ic}=20°C

In the CNT-based model, the temperature difference and open-circuit voltage between the p-type and n-type legs are approximately 1.5 to 2.5 times higher than those in the model without CNTs.

Fig. 7 illustrates the impact of leg width on both the temperature difference and the open-circuit voltage of the device. As shown, increasing the leg width leads to a reduction in both parameters for TE devices with and without CNTs, due to the enhanced rate of heat transfer throughout the legs. Similarly, the temperature difference and output voltage in the CNT-based model are about 1.5 to 2.19 times higher than in the model without CNTs. Consequently, TE device legs should ideally be tall and thin. However, the aspect ratio of the legs (height-to-width ratio) is constrained by fabrication technology and the chosen TE material.

Fig. 8 presents the effect of inlet fluid Reynolds number (or inlet velocity) at the heat source and sink channels on the hot and cold junctions for both models. The inlet air temperatures at the hot and cold channels are 37°C and 20°C, respectively. As observed, increasing the fluid Reynolds number raises the leg temperature at the hot side while lowering it at the cold side, owing to the higher heat transfer coefficient across the channels and consequently increasing the TE performance.

The improvement in the heat transfer coefficient is clearly demonstrated in Fig. 9. As shown, the heat transfer coefficient at the hot and cold junctions in the second model is higher than in the first model. For instance, when the Reynolds number is 50.52, the heat transfer coefficient for the TE device with CNTs is 2.5 times greater than that of the device without CNTs.

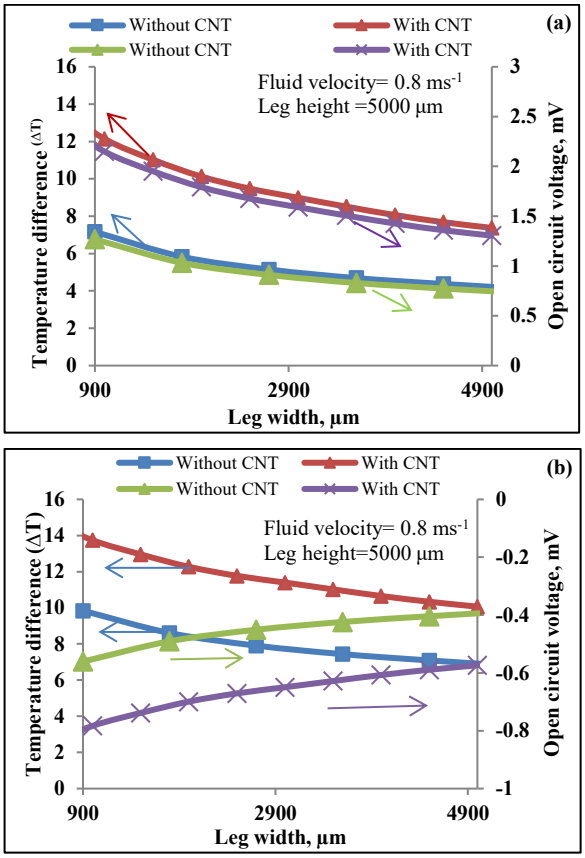

Fig. 7. The effect of legs width on the temperature differences and open circuit voltage for a given velocity for TE without and with CNTs (a) p and (b) n type legs. T_{ih}=37°C and T_{ic}=20°C

As previously mentioned, incorporating CNT microfins increases the effective heat transfer surface while simultaneously disrupting fluid flow. These combined effects significantly enhance the rate of heat transfer.

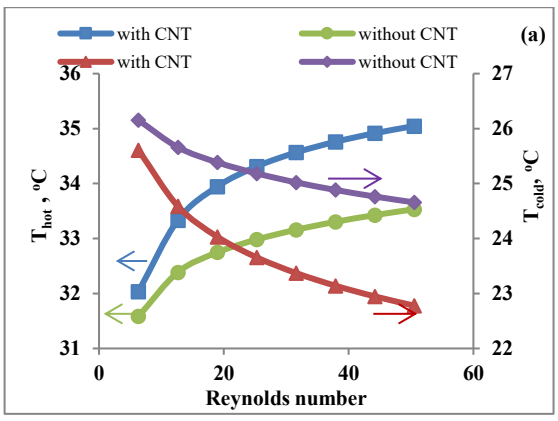

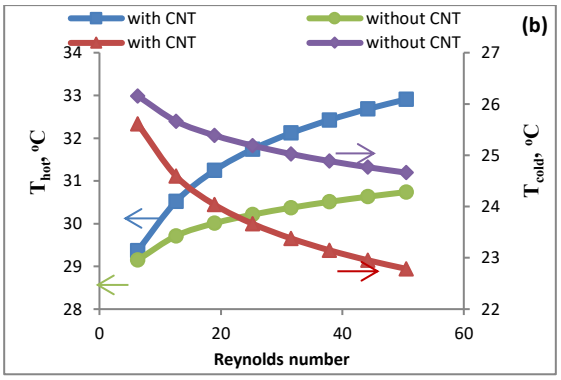

Fig. 8. Variations of temperature at two sides of (a) n and (b) p type legs versus Reynolds number for TE with and without CNT. T_{ih}=37°C and T_{ic}=20°C

A variable load resistance is connected to the TE device output to evaluate its generated power. Fig. 10 illustrates the power variations as a function of load resistance for both the first and second models. Maximum power is achieved when impedance matching occurs—that is, when the load resistance equals the total electrical resistance, allowing optimal power transfer from the device to the load.

Using this curve, the optimal internal electrical resistance of the device can be determined. By configuring a specific number of TE devices in series or parallel, the total electrical resistance of the TE system can be adjusted to match the consumer resistance, ensuring maximum power delivery. Additionally, the results indicate that the maximum power of the second model is 2.5 times higher than that of the first model, attributed to the incorporation of CNT microfins.

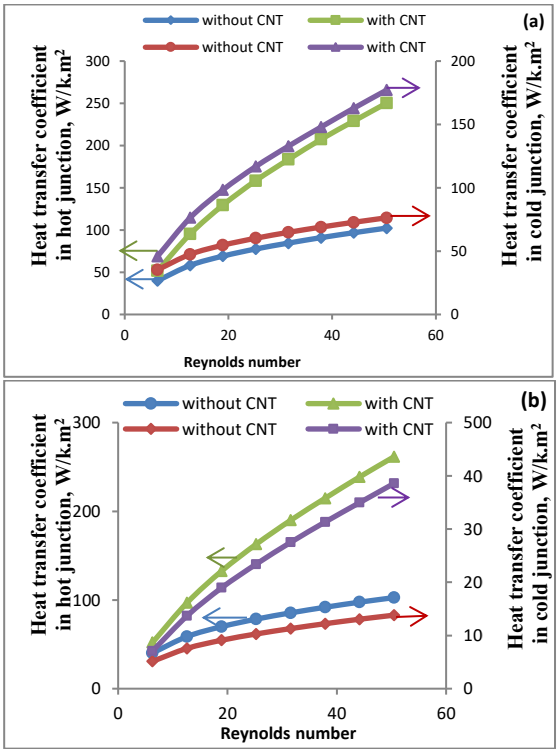

Fig. 9. Heat transfer coefficient of (a) n and (b) p type legs in hot and cold junctions versus Reynolds number for TE with and without CNTs. T_{ih}=37°C and T_{ic}=20°C

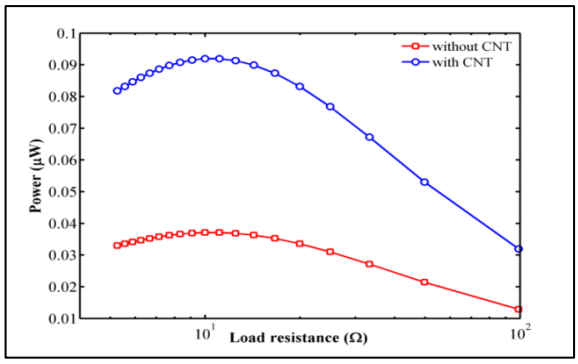

Fig. 10. Electrical power of TE device versus variable load resistance for the models with and without CNTs. Tih=37°C and Tic=20°C

Thermopile

In order to increasing the output voltage and power of a TE system, a thermopile has been considered. The thermopile consists of five TE devices that are electrically connected in series while being thermally arranged in parallel (see Fig. 11).

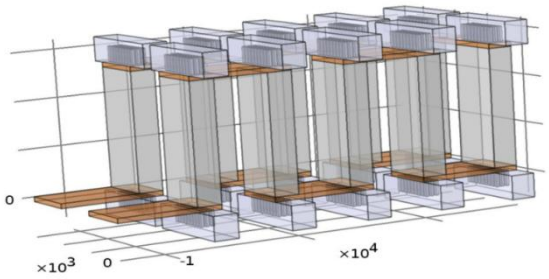

Fig. 11. 3D scheme of thermopile consists of 5 the TE devices with the micro fins CNT arrays on the both sides of the legs

Fig. 12 illustrates the temperature distribution along the TE legs in thermopiles with and without CNTs. A comparison of the two curves reveals that the temperature difference across the legs in the CNT-based model is 1.5 times greater than in the model without CNTs. This improvement is attributed to the effect of CNT microfins on the convective heat transfer coefficient.

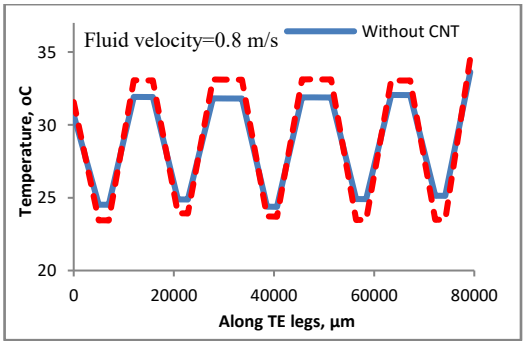

Fig. 12. Temperature distribution along TE legs in thermopile without and with CNT. Tih=37°C and Tic=20°C

Additionally, a variable resistance has been connected to the thermopile output. Fig. 13 illustrates the variations in thermopile power versus load resistance for two configurations: (a) without CNTs and (b) with CNTs. The

peak in both curves represents the internal electrical resistance of the thermopile, with maximum power transfer occurring when impedance matching is achieved.

According to Fig. 13, the total electrical resistance of the thermopile is 51.9 Ω. Furthermore, the maximum power of the CNT-based structure is twice that of the first model (without CNTs), owing to the inclusion of CNT microfins. The open-circuit voltage for the first and second models is measured at 8.6 mV and 12.047 mV, respectively, indicating that the voltage of the CNT-based model is 1.4 times higher than that of the first model.

A comparison of the calculated voltage and power between a single TE device and the thermopile demonstrates that connecting multiple TE devices enhances system output. By connecting five TE devices, the open-circuit voltage increases to 7 mV, while the output power rises to 0.3 μW. Therefore, integrating a greater number of TE devices can significantly improve the performance of TE systems.

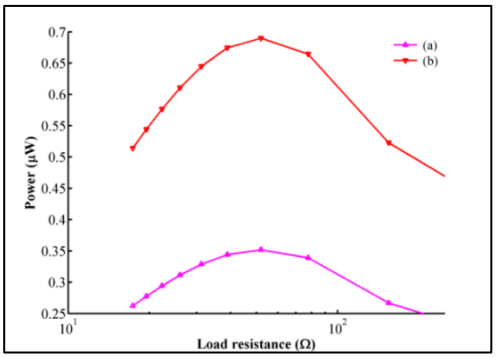

Fig. 13. Electrical power of thermopile versus variable load resistance, (a) without CNT and (b) with CNT. Tih=37°C and Tic=20°C

CONCLUSIONS

The performance of TE devices that harvest wasted thermal energy from fluid flow is numerically analyzed using the finite element method. Two polymeric TE device models are considered—one incorporating CNT arrays at the hot and cold source junctions, and the other without CNTs. The results indicate that, for a given Reynolds number and inlet air temperature at the heat source channels, the inclusion of CNTs leads to a greater temperature difference across both polymeric legs.

For both models, increasing the fluid Reynolds number enhances ΔT due to the rise in the heat transfer coefficient at the heat source channels, with this effect being more pronounced in the CNT-based device. Maximum power is achieved through impedance matching, which can be attained by configuring a specific number of TE devices in series or parallel.

The simulation results of a thermopile, composed of five interconnected TE devices, reveal that the open-circuit voltage and output power can reach up to 7 mV and 0.3 μW, respectively—approximately ten times the output of a single TE device. Additionally, the temperature difference across the thermopile legs in the CNT-based model is 1.5 times greater than that in the model without CNTs. Furthermore, the open-circuit voltage and maximum output power of the CNT-based thermopile increase by a factor of 1.4 to 2 compared to the non-CNT model.

ACKNOWLEDGMENT

The authors gratefully acknowledge Professor A. Behzadmehr for his valuable advice and consultations during the preparation of this manuscript.

REFERENCES

[1] V. Leonov, “Simulation of maximum power in the wearable thermoelectric generator with a small thermopile”, Microsyst. Technol., Vol. 17, No. 4, pp. 495–504, (2011). https://doi.org/10.1007/s00542-011-1234-5

[2] H. Lee, “Optimal design of thermoelectric devices with dimensional analysis”, Appl. Energy, Vol. 106, pp. 79–88, (2013). https://doi.org/10.1016/j.apenergy.2013.01.019

[3] A. Montecucco and A.R. Knox, “Accurate simulation of thermoelectric power generating systems”, Appl. Energy, Vol. 118, pp. 166–172, (2014). https://doi.org/10.1016/j.apenergy.2013.12.062

[4] L.E. Bell, “Cooling, heating, generating power, and recovering waste heat with thermoelectric systems”, Science, Vol. 321, No. 5895, pp. 1457–1461, (2008). https://doi.org/10.1126/science.1158899

[5] P. Górszczak, M. Rywotycki, S. Kąc, and M. Borówka, “Increase in the efficiency of electricity production with a thermoelectric generator (TEG)”, J. Therm. Anal. Calorim., (2023). https://doi.org/10.1007/s10973-023-12678-2

[6] T. Lu, Y. Li, J. Zhang, P. Ning, and P. Niu, “Cooling and mechanical performance analysis of a trapezoidal thermoelectric cooler with variable cross-section”, Energies, Vol. 13, No. 22, pp. 6070, (2020). https://doi.org/10.3390/en13226070

[7] B. Şişik and S. LeBlanc, “The influence of leg shape on thermoelectric performance under constant temperature and heat flux boundary conditions”, Front. Mater., Vol. 7, (2020). https://doi.org/10.3389/fmats.2020.598755

[8] A. Rjafallah, D.T. Cotfas, and P.A. Cotfas, “Legs geometry influence on the performance of the thermoelectric module”, Sustainability, Vol. 14, No. 23, pp. 15823, (2022). https://doi.org/10.3390/su142315823

[9] A. Ali, M.A. Zaheer, and N.M. Malik, “Design and simulation of thermoelectric generator to enhance the cooling rate and power generation from waste heat of chimney by employing different angles of flaps”, Eng. Proc., Vol. 23, No. 1, pp. 1–21, (2022). https://doi.org/10.3390/engproc2022023021

[10] W.A.N.W. Mohamed, N.F. Zamri, and M.F. Remeli, “Principal parameters of thermoelectric generator module design for effective industrial waste heat recovery”, J. Therm. Eng., Vol. 10, No. 2, pp. 457–478, (2024). https://doi.org/10.18186/thermal.1456700.

[11] A. Harb, K. Elsayed, A.E. Kabeel, M. Ahmed, and A. Abdo, “Investigating the modified thermoelectric

generator system performance", J. Therm. Anal. Calorim., Vol. 148, No. 21, pp. 11955–11968, (2023). https://doi.org/10.1007/s10973-023-12456-0

[12] H. Alghamdi, C. Maduabuchi, A. Albaker, I. Alatawi, T.R. Alsenani, A.S. Alsafran, et al., "A synergistic approach to optimizing the performance of a concentrating solar segmented variable area leg thermoelectric generator using numerical methods and neural networks", J. Therm. Anal. Calorim., Vol. 149, No. 11, pp. 5341–5365, (2024). https://doi.org/10.1007/s10973-024-12789-3

[13] Y.T. Lin, I. Permana, F. Wang, and R.J. Chang, "Improvement of heating and cooling performance for thermoelectric devices in medical storage application", Case Stud. Therm. Eng., Vol. 54, pp. 104017, (2024). https://doi.org/10.1016/j.csite.2023.104017

[14] D. Pang, A. Zhang, B. Wang, G. Li, and J. Lou, "A three-dimensional analytical model for performance evaluation of thermoelectric generators", Case Stud. Therm. Eng., (2024). https://doi.org/10.1016/j.csite.2024.105579

[15] P. Dziurdzia, P. Bratek, and M. Markiewicz, "An efficient electrothermal model of a thermoelectric converter for a thermal energy harvesting process simulation and electronic circuits powering", Energies, Vol. 17, No. 1, pp. 204, (2023). https://doi.org/10.3390/en17010204

[16] R. Kayabaşı and M. Kaya, "Effect of module operating temperature on module efficiency in photovoltaic modules and recovery of photovoltaic module heat by thermoelectric effect", J. Therm. Eng., Vol. 9, No. 1, pp. 191–204, (2023). https://doi.org/10.18186/thermal.1243519.

[17] S. Yang, H. Chen, and D. Luo, "A comprehensive review of thermoelectric generators from micropower supply to kilowatt system", Green Energy Fuel Res., (2025). https://doi.org/10.53941/gefr.2025.100008

[18] Y. Du, S.Z. Shen, K. Cai, and P.S. Casey, "Research progress on polymer–inorganic thermoelectric nanocomposite materials", Prog. Polym. Sci., Vol. 37, No. 6, pp. 820–841, (2012). https://doi.org/10.1016/j.progpolymsci.2011.06.007

[19] K. Xia, H. Zhan, Y. Wei, and Y. Gu, "Tensile properties of a boron/nitrogen-doped carbon nanotube–graphene hybrid structure", Beilstein J. Nanotechnol., Vol. 5, pp. 329–336, (2014). https://doi.org/10.3762/bjnano.5.38

[20] K. Kordás, G. Tóth, P. Moilanen, M. Kumpumäki, J. Vähäkangas, A. Uusimäki, et al., "Chip cooling with integrated carbon nanotube microfin architectures", Appl. Phys. Lett., Vol. 90, No. 12, (2007). https://doi.org/10.1063/1.2713755

[21] A.A. Balandin, "Thermal properties of graphene and nanostructured carbon materials", Nat. Mater., Vol. 10, No. 8, pp. 569–581, (2011). https://doi.org/10.1038/nmat3064

[22] W. Glatz, S. Muntwyler, and C. Hierold, "Optimization and fabrication of thick flexible polymer based micro thermoelectric generator", Sens. Actuators A Phys., Vol. 132, No. 1, pp. 337–345, (2006). https://doi.org/10.1016/j.sna.2006.02.008

[23] Y. Sun, P. Sheng, C. Di, F. Jiao, W. Xu, D. Qiu, et al., "Organic thermoelectric materials and devices based on p- and n-type poly(metal 1,1,2,2-ethenetetrathiolate)s", Adv. Mater., Vol. 24, No. 7, pp. 932–937, (2012). https://doi.org/10.1002/adma.201103118

[24] R.Y. Nuwayhid, M.S. Rahal, Y.Z. Makarem, and R.R. Achkar, "Thermal analysis of photovoltaic-thermoelectric hybrids", J. Therm. Eng., Vol. 10, No. 5, pp. 1149–1163, (2024). https://doi.org/10.14744/thermal.0000858.

[25] M.A.I. Rashid, M.F. Ismail, and M. Mahbub, "CFD analysis in a liquid-cooled carbon nanotube based micro-channel heatsink for electronic cooling", Int. J. Eng. Technol., Vol. 3, No. 5, pp. 553–559, (2011). https://doi.org/10.7763/IJET.2011.V3.284

[26] D. Mandic, "Numerical simulation of fluid flow and heat transfer through channels of plate heat exchangers", J. Fluid Flow Heat Mass Transf., Vol. 5, pp. 71–77, (2018). https://doi.org/10.11159/jffhmt.2018.007

[27] Z. Mo, R. Morjan, J. Anderson, E.E.B. Campbell, and J. Liu, "Integrated nanotube micro-cooler for microelectronics applications", IEEE Electron. Compon. Technol. Conf., Vol. 1, pp. 51–54, (2005).

[28] R. Cross, "Processing vertically aligned carbon nanotubes for heat transfer publications", Ph.D. Thesis, Georgia Institute of Technology, (2008).

[29] J. Liu, L.M. Zhang, L. He, and X.F. Tang, "Synthesis and TE properties of polyaniline", Wuhan Univ. Technol.-Mater. Sci. Ed., Vol. 18, pp. 53–55, (2003).

[30] M. Amrithesh, P.A. Francis Xavier, V.G. Chandraprabhu, S. Jayalekshmi, S.T. Lee, and J. Ravi, "Thermal diffusivity measurements in PANI and PANI-MWNT composites using photo acoustic technique", Trans. Indian Inst. Met., Vol. 64, No. 1–2, pp. 133–136, (2011). https://doi.org/10.1007/s12666-011-0072-1

[31] R. Vullers, R. van Schaijk, I. Doms, C. Van Hoof, and R. Mertens, "Micropower energy harvesting", Solid-State Electron., Vol. 53, No. 7, pp. 684–693, (2009). https://doi.org/10.1016/j.sse.2008.12.011

[32] M. Ruoho, "Nanostructured thermoelectric materials", Ph.D. Thesis, Aalto Univ. Sch. Electr. Eng., (2012).

[33] X.C. Xuan, K.C. Ng, C. Yap, and H.T. Chua, "A general model for studying effects of interface layers on thermoelectric devices performance", Int. J. Heat Mass Transf., Vol. 45, No. 26, pp. 5159–5170, (2002). https://doi.org/10.1016/S0017-9310(02)00205-2

[34] W. Wang, Y.T. Jin, Y.B. Zhu, X. Liao, H. Xu, H. Li, et al., "Structural design and manufacture of high packing density micro-thermoelectric power generators using thermoelectric films", IOP Conf. Ser.: Mater. Sci. Eng., Vol. 18, No. 14, pp. 142002, (2011). https://doi.org/10.1088/1757-899X/18/14/142002